Alkyl-Amino Functionalized Reduced-Graphene-Oxide–heptadecan-9-amine-Based Spin-Coated

physica status solidi b
www.pss-b.com

Alkyl-Amino Functionalized Reduced-Graphene-Oxide–heptadecan-9-amine-Based Spin-Coated Microsupercapacitors for On-Chip Low Power Electronics

Agin Vyas, Simin Zare Hajibagher, Ulises Mendez Romero, R. K. Azega, Ergang Wang, Per Lundgren, Peter Enoksson, and Anderson D. Smith*

With the miniaturization of microelectronics, integrated circuits can benefit from an on-chip solid-state power supply. Microsupercapacitors (MSCs), owing to their long lifetimes and complementary metal-oxide-semiconductor (CMOS) compatible fabrication, can be a potential on-chip energy storage unit. MSCs fabricated through spin coating graphene-oxide (GrO) often suffer from insufficient electrode thicknesses that lead to low energy densities. It, therefore, requires functionalizations for GrO that can improve the MSC electrode thickness and, thereby, the performance of the MSC. Thus, herein, the MSCs fabricated of alkyl-amino functionalized reduced-graphene-oxide–heptadecan-9-amine (rGO) are reported for enhanced electrode thickness, high capacitance, and lower series resistance compared with functionalized GrO-based MSCs (GO-MSCs). The functionalized rGO solves a significant issue of inadequate electrode thickness in wafer-scale MSC fabrication while achieving higher energy densities in fewer spin coatings. The rGO-MSC displays an areal capacitance of 108 μF cm^{-2} compared with 24 μF cm^{-2} for the GO-MSC while also demonstrating more than twice its power density in an integration compatible ionic liquid electrolyte 1-ethyl-3-methylimidazolium bis(trifluoromethylsulfony)imide (EMIM-TFSI).

1. Introduction

Wireless communications and digital electronics have led to the transmission of information through low cost and low power multifunctional miniaturized wireless sensor nodes.[1] These sensor nodes can transmit information from one node to another. An individual sensor node, shown in **Figure 1**a, comprises mainly four units—sensor, processor, transceiver, and power. For wireless nodes, the power supply must provide an output power of 100 μW to 10 mW to sustain functioning sensor, processor, and transceiver units. Traditionally, batteries are used as power supplies; however, their short life cycle and power density limit their utilization in wireless sensor nodes operating in areas that can be considered somewhat out-of-reach of human access. Therefore, we require a technology that can either entirely replace battery technology or complement its trade-off through advantages such as supercapacitors.

Supercapacitors are electrochemical double-layer capacitors that demonstrate high dynamic capacitance, and power density at low charging currents.[2] They also have extremely long lifetimes. These devices have emerged as possible candidates for on-chip energy storage in the form of complementary metal-oxide-semiconductor (CMOS) compatible spin-coated microsupercapacitors (MSCs).[3] MSCs are capable of powering low power, high-density microelectronics through on-chip integration with energy harvesting sources such as solar or vibrational harvesters fabricated through an integrated circuit (IC) compatible process, as shown in Figure 1b.[4] Recently MSCs have been fabricated through CMOS compatible technologies such as spray coating,[5] laser scribing,[6] chemical vapor deposition,[7] spin coating,[8] and ink-jet printing.[9] Among these techniques, spin coating is one of the few techniques that can be considered versatile in terms of device microfabrication resolution, utilization of a variety of electrodes, and heterogeneous integration of electrodes as discussed in our previous publication.[10]

Previous research in spin-coated MSC fabrication has utilized graphene-based material such as graphene oxide (GrO) as the material of choice for its high conductivity, surface area, and

A. Vyas, S. Zare Hajibagher, R. K. Azega, P. Lundgren, P. Enoksson
Micro and Nano Systems Group, (EMSL)
MC2, Chalmers University of Technology
Gothenburg 41258, Sweden
E-mail: agin@chalmers.se

U. Mendez Romero, E. Wang
Department of Chemistry and Chemical Engineering
Chalmers University of Technology
Gothenburg 41258, Sweden

A. D. Smith
Department of Electrical Engineering, E2
Chalmers University of Technology
Gothenburg 41258, Sweden

The ORCID identification number(s) for the author(s) of this article can be found under https://doi.org/10.1002/pssb.202100304.

DOI: 10.1002/pssb.202100304

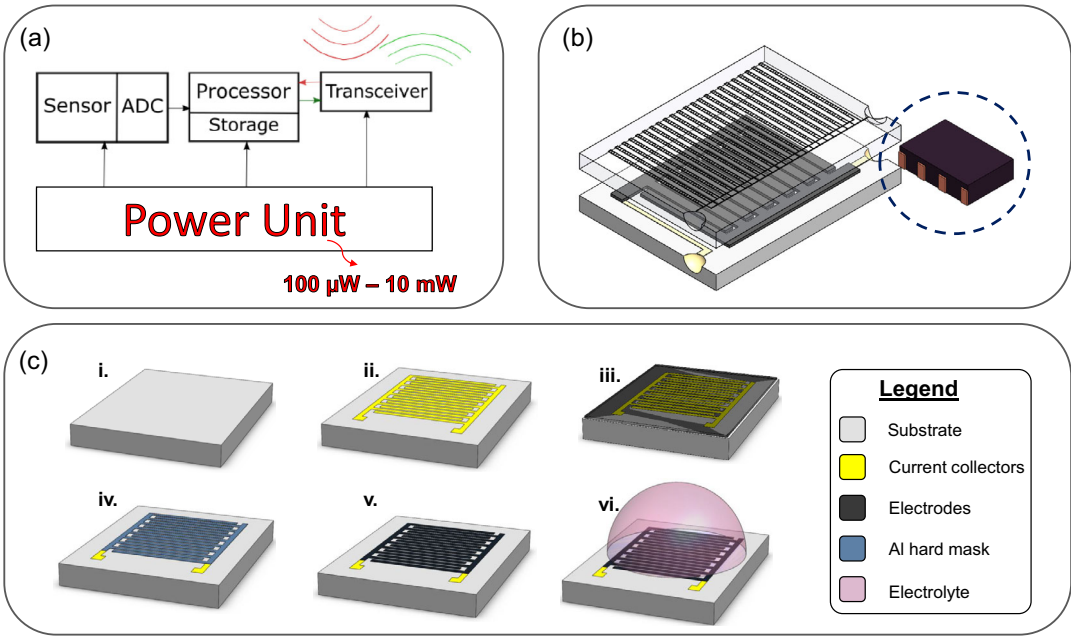

Figure 1. a) Schematic representation of an on-chip wireless sensor node. Sensors, processors, and transducers are powered by an energy storage unit such as a microsupercapacitor. Typically these devices need to provide from 10 μW to 10 mW of power. b) Microsupercapacitors can be integrated with energy harvester units such as photovoltaic cells or vibrational energy harvesters. The unit can be considered a power supply black box with input and output terminals in the blue inset. c) Fabrication process of microsupercapactors using GO and rGO solutions as materials for spin coating. Reproduced with permission.[21] Copyright 2019, Chalmers tekniska högskola.

versatility with pseudocapacitive material functionalization.[3] Even with improved surface uniformity and adhesion of reduced GrO (rGrO)-based electrodes, these devices cannot demonstrate high enough energy densities for on-chip integration application due to limited electrode deposition during spin coating. Therefore, we require functionalized GrO specifically synthesized for improving the resulting electrode thickness from spin coating deposition. Mendez et al.[11] have fabricated GrO functionalized with heptadecan-9-amine (abbreviated "GO" here), a branched alkane chain connected to the graphene flake's ends through a covalent bond, ending with an amine group for increased van der Waals adhesion between the deposited GO flakes during spin coating. This functional group prevents the graphene sheets from collapsing and also prevents agglomeration. GO is later reduced through hydrothermal treatment with ascorbic acid to form reduced functionalized GO (reduced-graphene-oxide–heptadecan-9-amine, abbreviated "rGO" here).

This article will discuss the performance of functionalized GO and rGO by fabricating MSCs comprised of these electrodes. The fabrication is performed through a CMOS compatible spin coating process that utilizes improved surface roughness for enhanced adhesion, uniformity, and coverage. The devices are characterized using a standard ionic liquid 1-ethyl-3-methylimidazolium bis(trifluoromethylsulfony)imide (EMIM-TFSI). The electrolyte is chosen for its high conductivity and ease of assembly in utilization in later packaging steps. The electrochemical measurements of the two electrodes are analyzed in the results section. The rGO has distinct advantages over GO in terms of high capacitance, energy, and power density with minor trade-offs in device resistance. The devices are also compared with GrO MSCs fabricated in our previous work.[10]

2. Experimental Section

2.1. Material Synthesis

Spin coating requires electrode material in solutions that have good dispersibility. To make graphene-based composite material solutions, we started the process by using graphene nanoparticle (GNPs) and performed the Hummer's process[12] to obtain aqueous solutions of GrO. The powder GNP (0.5 g) solution was oxidized in H_2SO_4 (30 ml) and KNO_3 (0.295 g) with $KMnO_4$ (3 g) after 6 h of reaction time while being stirred at 450 rpm at a temperature below 15 °C. The solution was quenched with DI water (100 mL) and H_2O_2 (30%, 6 mL). The yellow dispersion was centrifuged for 10 min at 3500 rpm with HCl (10%, 100 mL) added in the precipitate. The precipitate was centrifuged with DI water three times to obtain a higher purity. The recovered solution is mixed with DI water and stored as a solution. The functional group heptadecan-9-amine (HD9A) is mixed in ethanol and stirred with the solution with solvent at 450 rpm at room temperature for 5 min to achieve functionalized GO. The GO

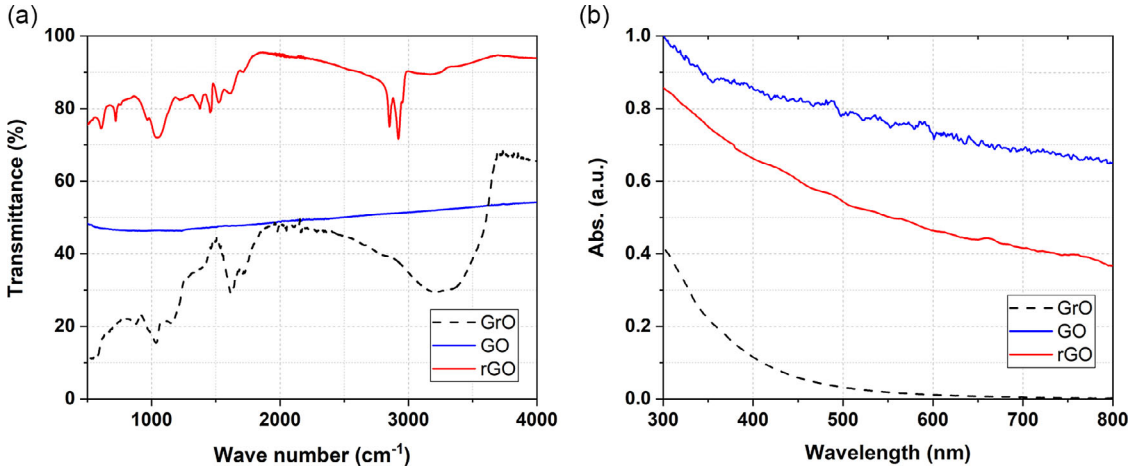

Figure 2. Characterization of of synthesized rGO, GO postannealing, and GrO in a) ATR-FTIR spectrum and b) UV–vis–NIR spectra.

solution is stored and used directly on the wafer substrate for MSC fabrication. GO-HD9A solutions were reduced to rGO using ascorbic acid-6-palmitate (100 mL) at 98 °C for 2 h at 450 rpm. The synthesized electrode materials are characterized using attenuated total reflection-Fourier-transform infrared spectroscopy (ATR-FTIR) (with PerkinElmer FTIR Spectrometer Frontier) for chemical modifications and UV–vis spectroscopy (PerkinElmer UV/vis/NIR Spectrometer Lambda 1050) for confirmation of complete reduction of the material in **Figure 2**.

2.2. Fabrication

The devices are fabricated using the processing scheme shown in Figure 1c. A silicon substrate is cleaned and the surface roughness is introduced as discussed in our previous research[8](Figure 1c-i using Cr (2 nm) layer as a roughening surface instead of Fe (4 nm). The current collectors—Au/Ti are evaporated on the substrate surface through a well defined lift-off process (Figure 1c-ii. The electrodes (GO and rGO) are spin coated at 500 rpm, five times (Figure 1c-iii) and vacuum dried. The electrodes are etched through an Al hard mask (Figure 1c-iv) and the hard mask and the roughening layers are etched (Figure 1c-v). Finally, the devices are coated with ionic liquid electrolyte EMIM-TFSI (Figure 1c-vi). For ease of reading, we will now call the two devices—GO-MSC and rGO-MSC. The GO-MSC is annealed at 500 °C in presence of Ar for 5 min to reduce the functionalized GrO. The heights of the electrodes measured using a profiler reveal a stark difference. The rGO-MSC has a thickness of 0.6 μm, while the GO-MSC has an electrode thickness of 0.1 μm. A more detailed fabrication process is explained in our previous publication.[8]

2.3. Characterization

The devices are characterized with EMIM-TFSI, an ionic electrolyte to measure the on-chip performance of MSCs from 0 to 1 V. The MSCs are electrochemically characterized for different scan rates from 20 to 5000 mV s^{-1}. The capacitance of the devices is calculated through

$$C = \frac{q}{2\Delta v} \tag{1}$$

where C is the capacitance, q is the charge, and Δv as the voltage window, and 2 in denominator represents the average of the q while charging and discharging. The energy of the devices is calculated from

$$E = \frac{C\Delta v^2}{2} \tag{2}$$

The charge–discharge experiments were conducted with a constant current from 1 to 20 μA cm^{-2}. The power is calculated from these experiments as

$$P = \frac{\Delta v^2}{4R_{esr}} \tag{3}$$

where R_{esr} is the device resistance from the IR drop in the charge–discharge curves. Impedance spectroscopy (EIS) measurements are conducted between 10 m and 10 MHz. The characteristic frequency (f_k),[13] is calculated as

$$\tau = 1/(f_k) \tag{4}$$

where f_k is the characteristic knee-point frequency of the MSC.

3. Results

3.1. Material Characterization

ATR-FTIR analysis is displayed in Figure 2a. It is well known that the GrO spectrum presents diverse oxygen functional groups: the typical broadband response from 3000 to 3700 cm^{-1} that refer to hydroxyl (OH) and carbonyl (C═O) at 1719 cm^{-1}. After annealing GO, synthesized from GrO, it resembles the typical graphite spectra.[14] It indicates that a chemical reduction has taken place. Similarly, in rGO, the prominent hydroxyl band is completely removed, as well as the carbonyl with the most perceptible bands for the two are at 2915 and 2850 cm^{-1} corresponding

to wavenumbers of C—H, respectively,[15] confirming a complete chemical reduction process.

The plot from UV–vis shown in Figure 2b demonstrates a linear dispersion in all the spectra, which is in agreement with the Dirac's electrons explained by the fine structure constant in graphene.[16] It corroborates that the sample was highly reduced and chemically derived into graphene rather than GrO. The absorbance of rGO follows a different behavior when compared to GrO, i.e., zero absorbance at greater wavelengths than 700 nm. This behavior could be attributed to rGOs because of the linear dispersion by Dirac's electrons,[17] which is also good evidence of a highly reduced graphene oxide, with recovered sp^2 hybridization that resembles a more graphene-like material instead of GO. Further information on the synthesis and characterization of the material can be found in the article reported by Mendez et al.[11]

3.2. Device Performance

The cyclic voltammograms in **Figure 3**a,b demonstrate the capacity of the electrode material to store charge at a constant voltage scan rate. In Figure 3a, the GO-MSC shows a capacitive behavior with a figure of merit $R = 0.7$; where R is the ratio of total charge stored (area under the current curve over a certain scan rate) and ideal capacitor storage capacity (area of the maximum current amplitude over a voltage range). At lower scan rates, the capacitive behavior is more pronounced due to the accessibility of the electrolyte ions in the electrode matrix. While at higher scan rates, the resistive response is dominating due to inaccessibility of ions to penetrate at faster switching of polarities. The rGO-MSC cyclic voltammograms, on the other hand, show an $R = 0.3$. This property demonstrates that the GO-MSC has a stronger capacitive behavior compared with rGO-MSC. In the cyclic voltammogram, the rGO-MSC shows a higher charge

Table 1. Equivalent circuit values for CPE-diff model for fabricated GO- and rGO-MSCs.

Component	GO	rGO	Units
R_u	98	221	Ω
Y_0	1.3 μ	2.5 μ	$S.s^{\alpha_0}$
α_0	0.82	0.85	—
W_d	0.7 μ	1.2 μ	$S.s^{0.5}$
R_p	12 M	1.3 k	Ω

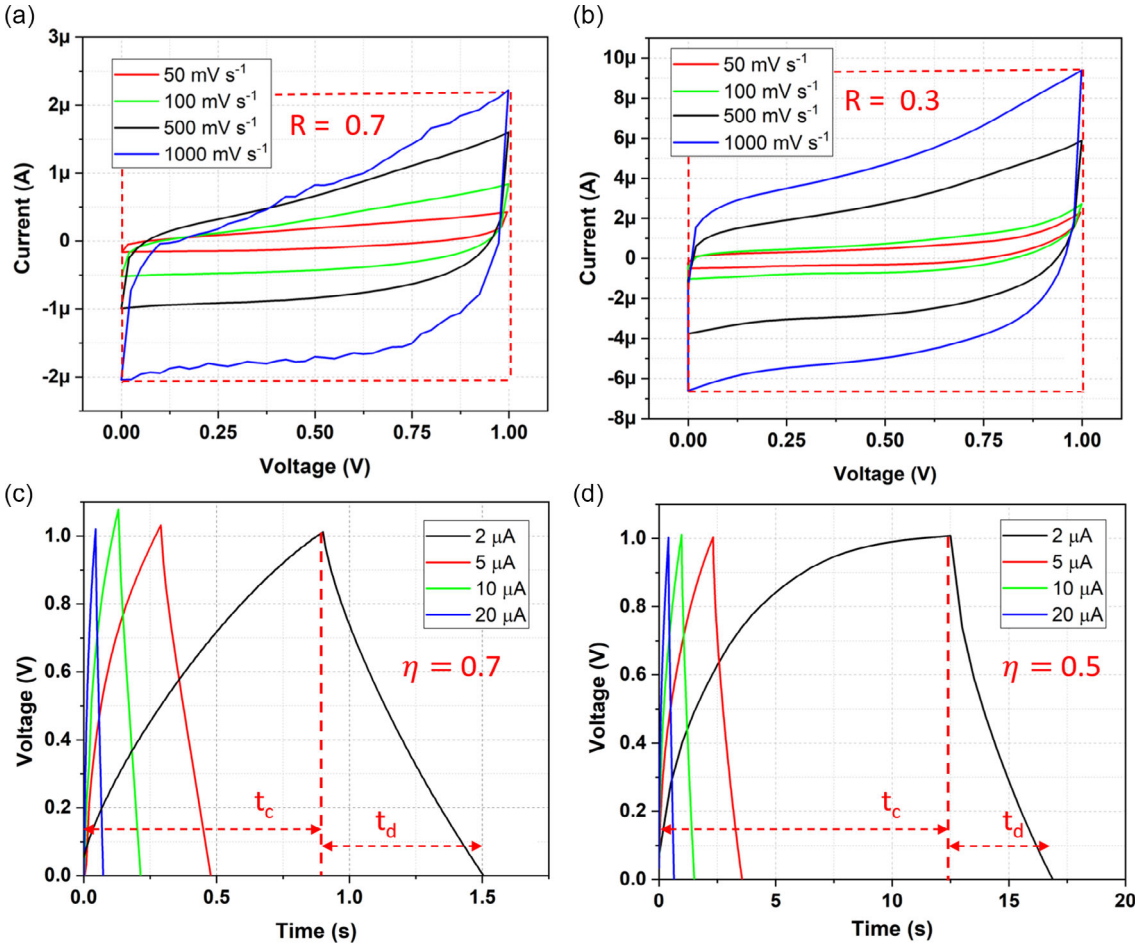

Figure 3. Electrochemical characterization of the fabricated MSCs. Cyclic voltammograms of a) GO- and b) rGO-MSC at 20 and 200 mV s^{-1}. GCD measurements for charging and discharging MSCs at constant current density for c) GO- and d) rGO-MSC.

storage capacity compared with GO-MSC. The larger charge storage capacity is mainly due to the thicker electrodes present on the rGO-MSC current collectors during spin coating.

The galvanostatic charge–discharge measurements of the GO- and rGO-MSCs are shown in Figure 3c,d, respectively. As observable, the rGO-MSC takes a considerably longer time to charge entirely to 1 V, especially at 2 μA cm^{-2}. The slow charging correlates with the higher leakage current for rGO (i.e., lower parallel resistance, see **Table 1**). The large IR-drop at discharging is the fingerprint of the series resistance. The nonlinearity shows the presence of a leakage current that restricts the charging speed. The issue can be critical for low current producing harvesters. At higher charging currents, the devices demonstrate quasi ideal capacitive behavior. The Coulombic efficiency (η) of the devices are calculated as the ratio between the discharging (t_d) and charging (t_c) times. Analysis of galvanostatic charge–discharge cycles in Figure 3c,d exhibits a smaller IR drop across the rGO-MSC over GO-MSC.

The device performance can be examined further through investigation of charge retention in areal capacitance of fabricated MSCs at varying scan rates in **Figure 4**a and current densities in Figure 4b. rGO-MSC has poor charge retention compared with GO-MSC. The alkane functional group at the edges of rGO flakes causes steric hindrance in the ionic transportation of charges. This can adversely effect the rate of ion exchange in the smaller pores of the electrode material. Better charge retention in GO-MSC highlights the importance of the annealing process in reducing functionalized GO. The annealing under Ar flow at 500 °C reconfigures the defect content to improve π–π conjugated networks in graphene.[18] The improved networks allow for ion transportation at higher scan rates and current densities. The space between the sheets, provided by the attached functional groups, facilitates the movement of electrolyte molecules between the sheets and results in higher adsorption of charge carriers and consequently higher concentrations of stored electrons at the surface. Similar charge retention properties for rGO- and GO-MSC are observed in Figure 4b, where we see the areal capacitance of the devices at different charging current densities.

The EIS spectra in Figure 4c further illustrate the increased conductivity of the GO-MSC. The equivalent series resistance for rGO-MSC is 0.2 kΩ while the GO-MSC is 0.1 kΩ. At a glance, the porosity of rGO-MSC seems higher. This is observed through the slope of the low-frequency response curve. The GO-MSC shows two slopes in its frequency response, suggesting a higher parasitic charge transfer resistance. These observations are

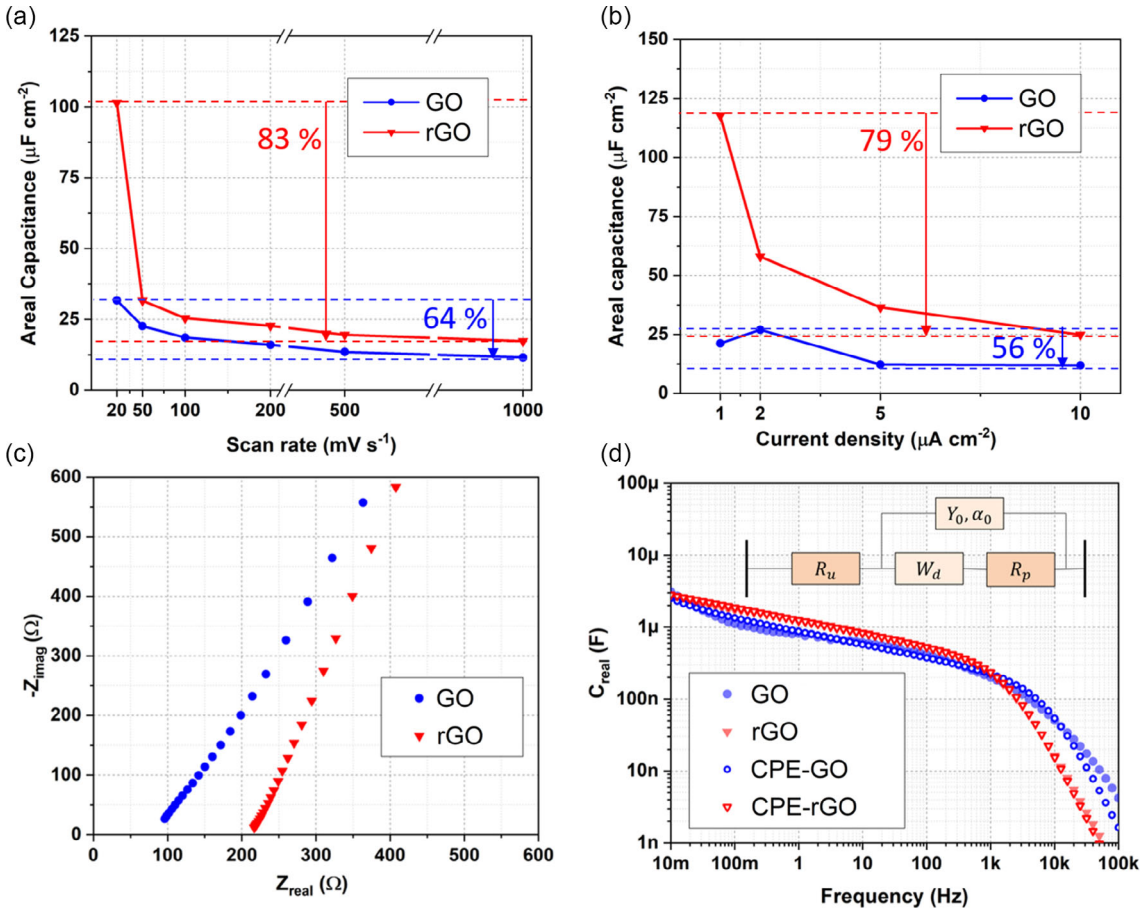

Figure 4. a) Calculated areal capacitance of the MSCs at scan rates from 20 to 1000 mV s^{-1}. b) Areal capacitance of the MSCs at varying current densities. c) Nyquist plot of the GO- and rGO-MSCs. The close to vertical line demonstrates a high porosity in the electrode material. d) Bode plot of the MSCs with CPE-diff model in the inset. The derived values from the equivalent circuit analysis are shown in Table 1.

validated on analyzing the device performance via equivalent circuit analysis of the Bode response shown in Figure 4d. The standard CPE-diff, constant phase element with diffusion coefficient, described by Bisquert et al.,[19] shown in the inset, is used to model the devices. The model has been explained in Huang et al[20] to model similar materials. A concise summary of results of individual elements can be found in Table 1. In Table 1, R_u is the resistance measured at the electrode–electrolyte interface; Y_0 is the constant phase element with a porosity coefficient in impedance at α; W_d is the Warburg impedance; and R_p is the parasitic resistance. The Bode response of both devices is quite similar visually; however, after inspection of the equivalent circuit analysis, we see a high parasitic resistance in GO-MSC. The parasitic leakage for the rGO is higher due to the low R_p—and that the implication of this is seen most clearly in Figure 4d with the distorted charging at low currents. The hump at low frequency in the Bode plot can attribute to the charge transfer through the parasitic resistance rather than stored in the device to its optimal capacity. The characteristic frequencies of GO- and rGO-MSCs are 5.3 and 8.3 kHz, respectively, with $\tau = 0.18$ and 0.12 ms.

4. Discussion

In this article, we demonstrate the performance of functionalized GrO with heptadecan-9-amine fixed at the outer edges at the GrO flakes. The electrode materials GO and rGO, distinguished from each other by the method of reduction, i.e., the former being reduced thermally post MSC fabrication and the latter reduced pre-fabrication, are spin coated on a silicon substrate with a current collector footprint of 0.13 cm^2. The summary of their device performances is shown in **Figure 5**, where we see a radar plot with different supercapacitor figure-of-merits. The rGO-MSC shows a high areal capacitance of 82 μF cm^{-2} at 50 mV s^{-1} while the GO-MSC has a capacitance of 24 μF cm^{-2} with the former having thicker electrodes. The energy density of rGO-MSC is higher than GO-MSC by a factor of 3. The power density of both devices is similar, however, rGO-MSC performs better in this aspect as well despite having a larger resistance in cyclic charge–discharge measurements. Finally, the resistance effects of electrode–electrolyte interface are larger in rGO-MSC.

Table 2. List of areal capacitance and power density measurements from the CV and GCD characterization of the GO-, rGO- and rGrO-MSCs.

Device	Areal capacitance [μF cm^{-2}]		Power density [mW cm^{-2}]	
Input signal	100 mV s^{-1}	1000 mV s^{-1}	2 μA cm^{-2}	5 μA cm^{-2}
Previous work[10]	112.0	72.5	12.8	5.5
GO	19	11.5	0.25	0.34
rGO	25	17.3	0.02	0.39

We also show a comparison of MSCs fabricated in this article with the results of the spin coated MSC fabricated in our previous article.[10] The MSC fabricated in the latter comprised of post reduced GrO, procured from Graphenea. The surface roughening agent used in the fabrication was Fe (4 nm) compared with Cr (2 nm) used in the current fabrication. The use of Cr as a surface roughening agent was determined due to its CMOS compatible nature and high melting point compared with Fe.[21] The devices are compared in terms of areal capacitance and power density in **Table 2** while the volumetric capacitance at varying scan rates is shown in Figure 5b.

As it can be seen in Table 2, both figures of merit are higher in the previous publication compared with the current work. The main reason behind depreciated performance in the current work can be attributed to procured thicknesses of the electrodes. The electrode thickness in the previous publication is 1.1 μm, while the thicknesses derived with GO- and rGO-MSCs are 0.1 and 0.6 μm, respectively, all after five turns of successive spin coatings. Contrasting these devices in terms of volumetric capacitance in Figure 5b, we see an improvement in the device performance for GO-MSC in comparison to rGO-MSC and MSC fabricated in the previous publication. Both the postannealed GrO-based MSCs—GO- and previous work MSC—retain their charge retention characteristics even at higher scan rates. The

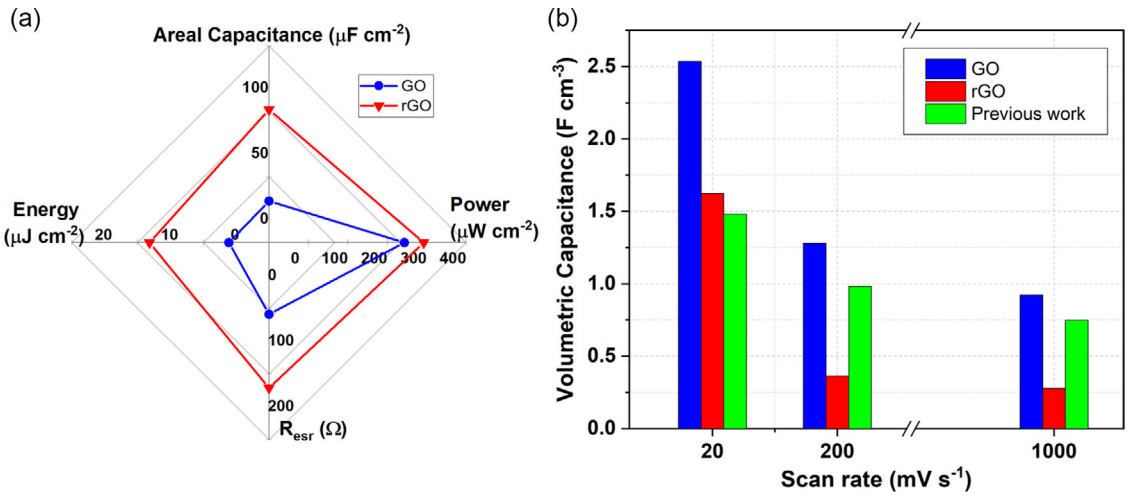

Figure 5. a) Radar plot for the fabricated GO- and rGO-MSC comparison. b) Comparison of volumetric capacitance of GO- and rGO-MSCs with our previously published work.[10]

rGO-MSC in comparison demonstrates a staggering drop in capacitance retention at higher scan-rates, as shown previously in Figure 4.

Combined with annealing and functionalization, GO-MSCs have a higher carbon-to-oxygen ratio compared with rGO-MSCs that has electrodes that were prereduced through ascorbic acid.[22,23] Furthermore, reducing GrO at high temperatures leads to an increase in specific surface area through reorientation of flakes to form structures of lowest entropy which increases the conductivity of electrodes and allows for faster charge–discharge at higher scan rates and current densities. The drop in volumetric capacitance of rGO-MSCs tends to remain constant over a range of higher scan-rates. This result can be perceived as a lack of penetration by the electrolyte ions into the inner regions of the electrode surface, that could have been accessed at low charging rates.

The spin-coated devices fabricated in this article lie within the range of expected values for GrO-based devices. GrO-based MSCs have been investigated extensively in literature in different configurations such flexible substrates, laser scribed circuits, and ink-jet deposited substrates. Gao et al.[24] fabricated MSCs based on rGO using laser-scribing demostrates the highest areal capacitance of 510 $\mu F\,cm^{-2}$ in presence of water as an electrotyle with GrO forming the ionic pathways between the interdigitated rGrO electrodes. Wu et al.[25] later demonstrated a high power density of 750 $\mu W\,cm^{-2}$ in presence of H_2SO_4/PVA electrolyte with a capacitance of 80 $\mu F\,cm^{-2}$. The group has also demonstrated performance of rGrO in presence of H_2SO_4 electrolyte with an high capacitance of 316 $\mu F\,cm^{-2}$ at 120 Hz frequency.[26] Niu et al.[27] demonstrated the performance of rGrO in presence of H_3PO_4/PVA. The device showed a capacitance of 462 $\mu F\,cm^{-2}$. Improvements in performance of GrO based MSCs can be achieved by synthesizing composites of materials with higher energy density or with synergistic specific surface areas with GrO. Wen et al.[28] produced GrO and carbon nanotube (CNT) composites to demonstrate 250 $\mu F\,cm^{-2}$. Recently, Boruah et al.[29] fabricated MSCs composed of rGrO mixed with V_2O_5 to produce 6 $mF\,cm^{-2}$. Later Mai et al.[30] utilized rGrO/CNT composites with MoS_2 to demonstrate a high energy density of 80 $mF\,cm^{-2}$. MoS_2 and V_2O_5 are a few examples of 2D materials that can be synthesized in a mixture with rGrO and utilized for fabricated for making spin-coated MSCs. However, as discussed previously, rGrO-based solutions cannot be effectively utilized for a scalable spin-coating process as the flakes tend to agglomerate in a standing solution; we require rGO-based solutions that cannot only fabricate robust stand-alone MSCs but also can be a viable alternate for nonfunctionalized rGrO without changing its inherent properties of conductivity.

5. Conclusion

Fabrication of wafer scale CMOS compatible GrO-based MSCs require thicker deposited electrodes to achieve high energy densities. The synthesized rGO functionalized with branched alkylamino groups provides a solution while retaining majority of GrO's electrical properties. In this article, we have demonstrated a scalable fabrication method to investigate the properties of rGO as electrodes for MSC. rGO-MSCs show capacitance of 0.1 $mF\,cm^{-2}$ at 20 $mV\,s^{-1}$, energy density of 54 $\mu J\,cm^{-2}$ at the same scan rate and power density of 0.3 $mW\,cm^{-2}$. The device is also compared with GO-MSC, which contains spin-coated GO annealed to rGO at 500 °C. The GO-MSCs demonstrates a capacitance of 34 $\mu F\,cm^{-2}$, 17 $\mu J\,cm^{-2}$, and 0.24 $mW\,cm^{-2}$ at the same inputs. The results demonstrate that pre-reduced rGO electrodes for MSCs not only reduce the thermal budget of the fabrication, but they also allow for improved electrode thickness which results in higher capacitance per unit area of the chip.

Acknowledgements

This project has received funding from the European Union's Horizon 2020 research and innovation programme under grant agreement No 101006963 (GreEnergy). The authors acknowledge the funding from the projects: Vinnova, Area of Advance (AoA) MESSIAH, and SAAB Hogeffektradar. The authors also thank Chalmers NanoFabLab for their cleanroom expertise and Dr. Jinhua Sun for his inputs.

Conflict of Interest

The authors declare no conflict of interest.

Data Availability Statement

The data that support the findings of this study are available from the corresponding author upon reasonable request.

Keywords

2D materials, CMOS compatible, energy storage, microsupercapacitors, functionalized reduced-graphene-oxide, heptadecan-9-amine, spin coating

Received: June 29, 2021
Revised: October 19, 2021
Published online:

[1] M. Dener, *Comput. Electric. Eng.* **2017**, *64*, 380.
[2] B. E. Conway, *Electrochemical Supercapacitors: Scientific Fundamentals and Technological Applications*, Springer Science & Business Media, Boston, MA **2013**.
[3] A. Smith, Q. Li, A. Vyas, M. M. Haque, K. Wang, A. Velasco, X. Zhang, S. Thurakkal, A. Quellmalz, F. Niklaus, K. Gylfason, P. Lundgren, P. Enoksson, *Sensors* **2019**, *19*, 4231.
[4] Q. Li, Ph.D. thesis, Chalmers Tekniska Hogskola (Sweden), **2018**.
[5] H. Huang, X. Chu, H. Su, H. Zhang, Y. Xie, W. Deng, N. Chen, F. Liu, H. Zhang, B. Gu, W. Deng, W. Yang, *J. Power Sources* **2019**, *415*, 1.
[6] C. Kim, D.-Y. Kang, J. H. Moon, *Nano Energy* **2018**, *53*, 182.
[7] A. Vyas, K. Wang, Q. Li, A. M. Saleem, M. Bylund, R. Andersson, V. Desmaris, A. Smith, P. Lundgren, P. Enoksson, *RSC Adv.* **2020**, *10*, 31435.
[8] A. Vyas, K. Wang, A. Anderson, A. Velasco, R. Van den Eeckhoudt, M. M. Haque, Q. Li, A. Smith, P. Lundgren, P. Enoksson, *ACS Omega* **2020**, *5*, 5219.
[9] C. Shen, C. P. Wang, M. Sanghadasa, L. Lin, *RSC Adv.* **2017**, *7*, 11724.
[10] A. Vyas, S. Z. Hajibagher, Q. Li, M. Haque, A. Smith, P. Lundgren, P. Enoksson, *Phys. Status Solidi B* **2021**, *258*, 2000358.

[11] U. A. Mendez-Romero, S. A. Pérez-Garca, X. Xu, E. Wang, L. Licea-Jiménez, *Carbon* **2019**, *146*, 491.
[12] W. S. Hummers Jr., R. E. Offeman, *J. Am. Chem. Soc.* **1958**, *80*, 1339.
[13] D. Pech, M. Brunet, H. Durou, P. Huang, V. Mochalin, Y. Gogotsi, P.-L. Taberna, P. Simon, *Nat. Nanotechnol.* **2010**, *5*, 651.
[14] M. Acik, G. Lee, C. Mattevi, M. Chhowalla, K. Cho, Y. Chabal, *Nat. Mater.* **2010**, *9*, 840.
[15] M. Badertscher, P. Bühlmann, E. Pretsch, *Structure Determination of Organic Compounds*, Springer Berlin Heidelberg, Berlin **2009**.
[16] R. R. Nair, P. Blake, A. N. Grigorenko, K. S. Novoselov, T. J. Booth, T. Stauber, N. M. Peres, A. K. Geim, *Science* **2008**, *320*, 1308.
[17] T. Carey, S. Cacovich, G. Divitini, J. Ren, A. Mansouri, J. M. Kim, C. Wang, C. Ducati, R. Sordan, F. Torrisi, *Nat. Commun.* **2017**, *8*, 1.
[18] P. Zhang, Z. Li, S. Zhang, G. Shao, *Energy Environ. Mater.* **2018**, *1*, 5.
[19] J. Bisquert, G. Garcia-Belmonte, P. Bueno, E. Longo, L. Bulhoes, *J. Electroanal. Chem.* **1998**, *452*, 229.
[20] J. Huang, Y. Gao, J. Luo, S. Wang, C. Li, S. Chen, J. Zhang, *J. Electrochem. Soc.* **2020**.
[21] A. Vyas, Licentiate Thesis, Chalmers University of Technology, **2019**.
[22] B. Zhao, P. Liu, Y. Jiang, D. Pan, H. Tao, J. Song, T. Fang, W. Xu, *J. Power Sources* **2012**, *198*, 423.
[23] K. K. H. De Silva, H.-H. Huang, M. Yoshimura, *Appl. Surf. Sci.* **2018**, *447*, 338.
[24] W. Gao, N. Singh, L. Song, Z. Liu, A. L. M. Reddy, L. Ci, R. Vajtai, Q. Zhang, B. Wei, P. M. Ajayan, *Nat. Nanotechnol.* **2011**, *6*, 496.
[25] Z.-S. Wu, K. Parvez, X. Feng, K. Müllen, *Nat. Commun.* **2013**, *4*, 2487.
[26] Z. Wu, L. Li, Z. Lin, B. Song, Z. Li, K.-S. Moon, C.-P. Wong, S.-L. Bai, *Sci. Rep.* **2015**, *5*, 1.
[27] Z. Niu, L. Zhang, L. Liu, B. Zhu, H. Dong, X. Chen, *Adv. Mater.* **2013**, *25*, 4035.
[28] F. Wen, C. Hao, J. Xiang, L. Wang, H. Hou, Z. Su, W. Hu, Z. Liu, *Carbon* **2014**, *75*, 236.
[29] B. D. Boruah, S. Nandi, A. Misra, *ACS Appl. Energy Mater.* **2018**, *1*, 1567.
[30] W. Yang, L. He, X. Tian, M. Yan, H. Yuan, X. Liao, J. Meng, Z. Hao, L. Mai, *Small* **2017**, *13*, 1700639.